Theoretical and Applied Fracture Mechanics 116 (2021) 103090

Contents lists available at ScienceDirect

Theoretical and Applied Fracture Mechanics

journal homepage: www.elsevier.com/locate/tafmec

DIC-based structural strain approach for low-cycle fatigue assessment of AA 5083 welded joints

Pasqualino Corigliano [a,*], Vincenzo Crupi [a], Xianjun Pei [b], Pingsha Dong [b]

[a] Department of Engineering, University of Messina, Contrada di Dio - 98166 - Sant'Agata, Messina, Italy
[b] Department of Naval Architecture and Marine Engineering, University of Michigan, Ann Arbor, MI 48105, United States

ARTICLE INFO

Keywords:
Low-cycle fatigue
Welded joints
Ship structures
Digital image correlation structural strain approach
Finite element structural strain approach

ABSTRACT

The aim of this research was the development and application of the following structural strain approaches for predicting the low-cycle fatigue life of AA 5083 welded joints: Finite Element equivalent structural strain approach and Digital Image Correlation equivalent structural strain approach. The first one was already applied for the low-cycle fatigue life prediction of welded joints, while the second approach is here proposed for the first time.

Low-cycle fatigue tests were conducted at displacement ratios equal to minus one and zero.

The Digital Image Correlation technique was used to analyze the local behaviour in proximity of the welded fillet and to obtain a notch equivalent strain range–number of cycles curve.

Furthermore, a complete indipendent experimental procedure to evaluate the equivalent structural strain range, using the Digital Image Correlation technique, was proposed.

A Finite Element analysis, with the advantage of being mesh insensitive and requiring only the elastic parameters, was performed in order to apply the Finite Element equivalent structural strain approach.

The two structural strain approaches were used to predict the fatigue life, obtainining good agreement with the ASME mean curve representing over 1000 experimental data.

1. Introduction

Several approaches have been developed for the fatigue assessments of welded joints and a review is provided by Fricke [1].

The simplest and easiest method is the nominal stress approach [2], which does not take into account local stress increases due to structural discontinuity (as a stiffener end) and local weld profile.

The structural hot-spot stress approach [3,4] includes all stress concentration effects of a welded joint except the one due to the local weld toe.

The effective notch stress approach using the fictitious notch radius [5,6] contemplates the increase in local stress at the notch produced by the weld toe or the weld root and is based on the theory of elasticity, without considering the elastic–plastic material behavior.

The notch stress intensity factor approach [7,8] is generally used to assess the crack initiation at sharp corners and takes into account notch opening angle (weld toe angle in case of welded details) and notch tip radius (or weld toe radius), starting from the nominal or structural stresses in the notched structural member.

The Critical Distance Methods (CDMs) [9-12] are based on the assumption that the failure of a structure occurs when the fatigue limit is surpassed within a region surrounding the notch (critical volume or length). CDMs were successfully applied for the fatigue prediction of welded joints in [10,13,14].

The thermal methods [15-18] are based on the self-heating effect during fatigue loading, which is closely related with microstructural changes [19], and were successfullly applied for the fatigue prediction of welded joints in [13,15,16,20,21].

Energy approaches, such as averaged strain energy density (SED), were also applied for the fatigue assessment of welded joints [22-24]. A review of the volume-based SED approaches applied to welded structures is provided in [25].

The notch strain approach [26] considers the effect of the elastic–plastic stress/strain relationship in the notch on the fatigue strength and the cyclic stress/strain curve is generally used to perform non-linear FE analyses in low-cycle fatigue (LCF) conditions.

The crack propagation approach is applied when the fatigue strength and service life of an existing crack or crack-like defect, needs to be determined [27], so this approach can be seen as a supplement of the

* Corresponding author.
E-mail addresses: pcorigliano@unime.it (P. Corigliano), crupi.vincenzo@unime.it (V. Crupi), xpei@umich.edu (X. Pei), dongp@umich.edu (P. Dong).

https://doi.org/10.1016/j.tafmec.2021.103090
Received 7 July 2021; Received in revised form 30 August 2021; Accepted 30 August 2021
Available online 2 September 2021

Nomenclature

$\mathbf{d_a}$:	displacement amplitude
$\mathbf{d_{max}}$:	maximum displacement
$\mathbf{d_{min}}$:	minimum displacement
f :	frequency
$\boldsymbol{m}$:	fracture mechanics parameter
$\boldsymbol{r}$:	bending ratio
$\boldsymbol{t}$:	thickness of the plate
$\boldsymbol{t^*}$:	thickness ratio
$\boldsymbol{t_{ref}}$:	thickness of reference
$\boldsymbol{y_i}$:	y coordinate at the *ith* node
$\boldsymbol{E}$:	Young's modulus
$\boldsymbol{F_i}$:	nodal force at the *ith* node
$\boldsymbol{I(r)}$:	life integral
$\mathbf{N_i}$:	number of cycles to crack initiation
$\mathbf{R_d}$:	displacement ratio ($R_d = d_{min}/d_{max}$)
$\boldsymbol{\epsilon_b}$:	bending strain
$\boldsymbol{\epsilon_m}$:	membrane strain
$\boldsymbol{\epsilon_s}$:	structural strain
$\boldsymbol{\epsilon_{s\_max}}$:	maximum structural strain
$\boldsymbol{\epsilon_{s\_min}}$:	minimum structural strain
$\boldsymbol{\varepsilon_x}$:	strain in the x direction
$\boldsymbol{\varepsilon_y}$:	strain in the y direction
$\boldsymbol{\varepsilon_{xy}}$:	strain in the xy direction
$\boldsymbol{\varepsilon_{DIC}}$:	equivalent strain measured by the DIC technique
$\boldsymbol{\varepsilon_1}$:	first principal strain
$\boldsymbol{\varepsilon_2}$:	second principal strain
$\boldsymbol{\varepsilon_3}$:	third principal strain
$\boldsymbol{\nu}$:	poisson modulus
$\boldsymbol{\sigma_b}$:	normal bending stress
$\boldsymbol{\sigma_m}$:	membrane stress
$\boldsymbol{\Delta E_s}$:	equivalent structural strain range evaluated from Finite Element analysis
$\boldsymbol{\Delta E_{s\_DIC}}$:	equivalent structural strain range evaluated from Digital Image Correlation analysis
$\boldsymbol{\Delta\varepsilon_{n\text{-}DIC}}$:	notch strain range evaluated from Digital Image Correlation analysis
$\boldsymbol{\Delta\epsilon_s}$:	structural strain range
$\boldsymbol{\Delta\epsilon_{s\_DIC}}$:	structural strain range evaluated from Digital Image Correlation analysis

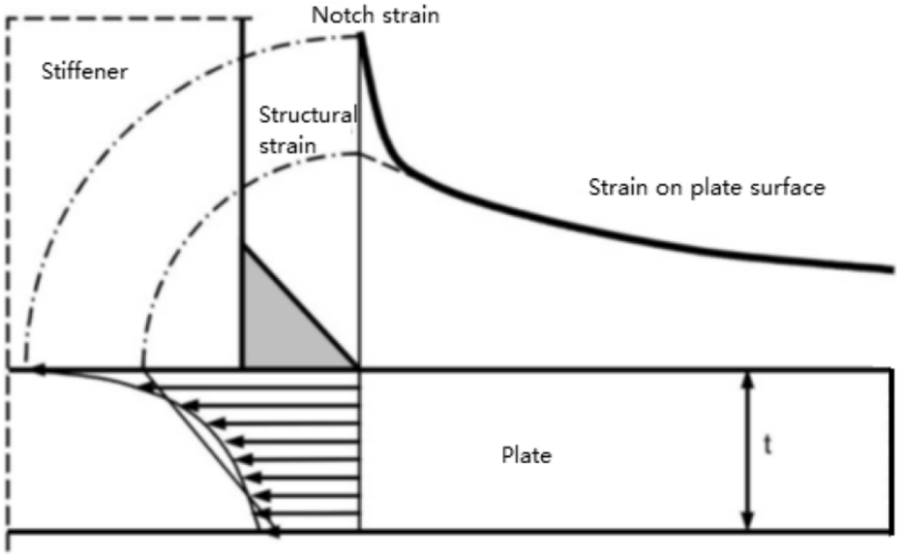

Fig. 1. Structural strain and notch strain definition.

aforementioned methods.

The traction structural stress/strain approach [28] was specifically developed for the fatigue behavior of welded structural details in which notch radii are ill-defined [4,28-32]. One of the main advantages is represented by the fact that the structural strain method is mesh-insensitive. Furthermore, fatigue data can be correlated with a single master S-N/E-N curve (the latter is valid both in high and low cycle fatigue regimes) without weld classification approaches.

Most ship structures consist of plate details, connected to longitudinal and transverse members by welded joints, which are sites of high-stress concentrations, and are subject to extreme wave loading during severe weather conditions, such as storms, ship motions, and loading/unloading operations, which induce significant fatigue loads [33,34]. The presence of stress concentrations and fatigue loads leads to cyclic stress that exceeds the yield stress locally.

Summing these effects to the presence of welding complicates, even more, the problems. Thus, ship hull structures could suffer from LCF loadings and the plastic deformation accumulation phenomenon may occur, leading to fatigue failures particularly at welded joints. A ship, damaged by collision or grounding, could encounter large wave amplitudes during the salvage period, causing in some parts of the structure cyclic plasticity and fatigue crack propagation as a consequence of LCF process [35].

Residual stresses are also a in importact factor that influences the fatigue life. Some studies have shown an improvement of the fatigue life using treatments that generate compressive residual stresses [36]. However, as reported in [37,38], they mainly have to be considered when dealing with high-cycle fatigue (HCF) loadings. Indeed, it is often contemplated that they are relaxed due to the high loads and plasticity levels induced during the LCF life and, especially for fatigue lifespans under 10,000 cycles, the initial stress influence disappears obtaining similar fatigue lifespans for all initial states [37].

The aim of this research activity was to predict the LCF life of AA 5083 welded joints, widely used for shipbuilding, applying two

Fig. 2. Deck panel made of AA 5083.

Table 1a
Chemical composition evaluated by XRF.

Test	Si	Mg	Fe	Cr	Al
	%	%	%	%	%
1	0,12	3,42	0,14	0,11	95,8
2	0,14	3,84	0,14	0,12	95,3
Mean	0,13	3,63	0,14	0,11	95,6
St. Dev.	0,036	0,6	0,007	0,009	0,63

Table 1b
Mechanical properties of the investigated Al alloy.

Vickers Hardness	Ultimate Tensile Strength MPa	Tensile Yield Strength MPa	Elongation at Break %	Modulus of Elasticity MPa
96	317	228	16	71,000

approaches: Finite Element equivalent structural strain approach and Digital Image Correlation equivalent structural strain approach.

Some of the authors have already applied the Digital Image Correlation (DIC) technique to aluminum/steel explosive welded joints under bending loading [39] and anaerobic adhesives under high pressure and torque loading [40].

In this investigation, the DIC technique was used to analyze the local behaviour in proximity of the welded fillet. In addition, a complete independent experimental procedure to evaluate the equivalent structural strain range ($\Delta\varepsilon_{s\text{-}DIC}$), using the DIC technique, was proposed for the first time.

The other authors have already developed the Finite Element equivalent structural strain approach [28,32]. Thus, a Finite Element analysis (FEA) of the investigated joint was performed and the structural strain approach, was applied. The equivalent structural strain range (ΔE_s) was evaluated and correlated to the number of cycles in order to obtain a $\Delta E_s - N$ curve.

The structural strain values were calculated in the plate surface experimentally and on the plate thickness by means of FE calculations, as reported in Fig. 1. The obtained results were then compared to the ASME Div 2 master E-N curve [30].

2. Experiments

2.1. Specimen and testing procedure

The most used aluminum alloys in corrosive environments, such as sea water, are the 5000 and 6000 series alloys, which provide adequate strength and excellent corrosion resistance. The investigated specimens, made of AA 5083 and welded by means of the MIG process, were provided by a shipyard. Fig. 2 shows a deck panel made of welded of AA 5083. Table 1a reports the X-Ray Fluorescence (XRF) test results of the chemical composition performed using a SPECTRO xSORT machinery which supplies elemental testing and spectrochemical analysis of materials and Table 1b reports the mechanical properties of the investigated alloy parent metal. Fig. 3 shows the geometrical dimension (width equal to 24,5 mm). Failure is expected in correspondence of toe fillets (welds A and B) or toe plate (weld C), as indicated in Fig. 3(c).

LCF tests were performed under displacement amplitude control (d_a) applying two displacement ratios: $R_d = -1$ and and $R_d = 0$, with the aim of investigating how the mean strain could affect the LCF life of the specimens. Furthermore, LCF tests at $R_d = -1$ with $d_a > 0.35$ mm were excluded from the present analysis due to the onset of buckling during compressive loading. The residual stress effect was neglected because, as mentioned, they mainly influence the HCF life rather than the LCF life

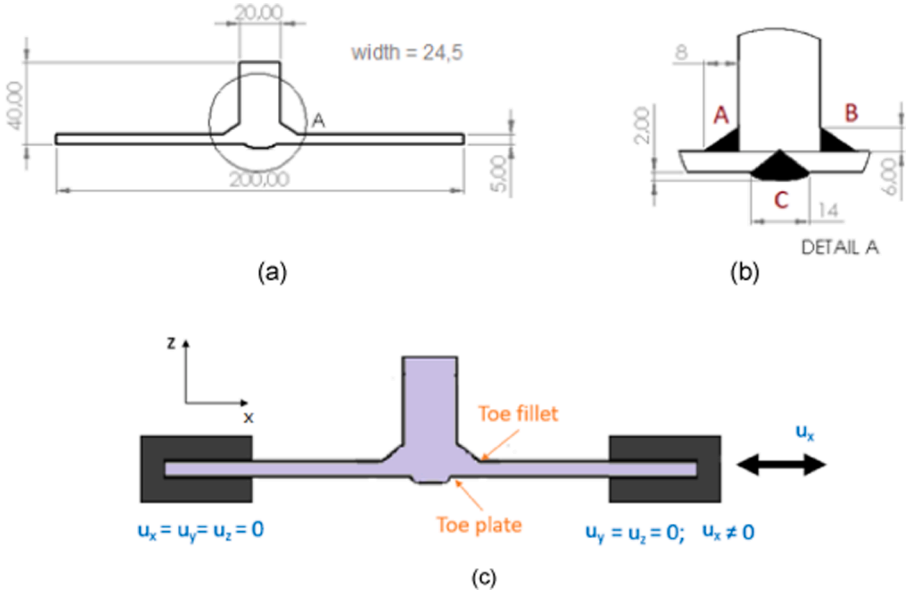

Fig. 3. Geometry of the tested specimens. (Units are in mm).

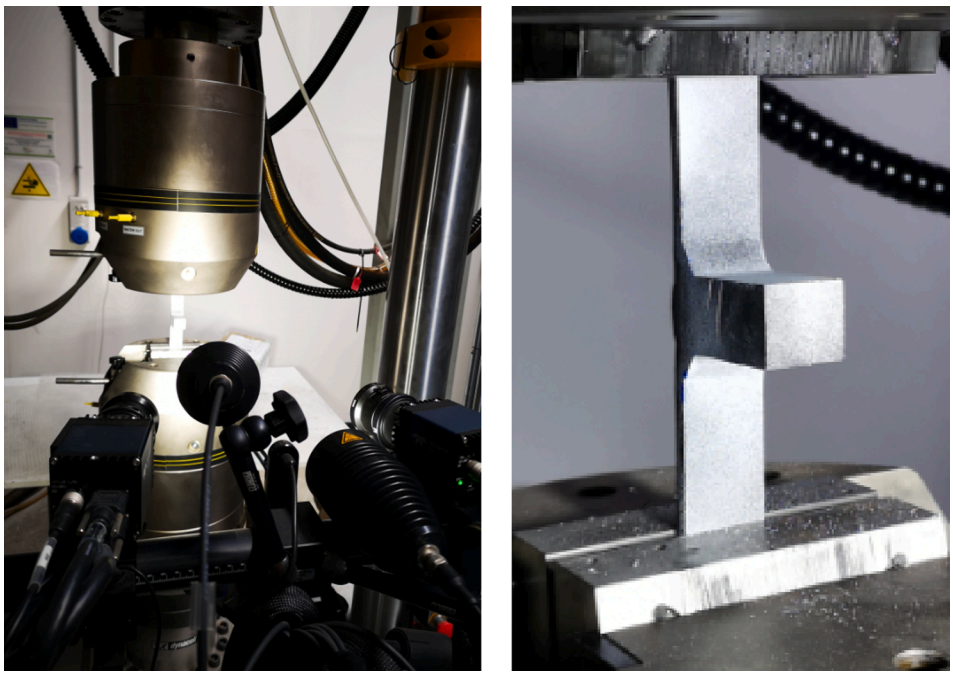

Fig. 4. Experimental setup.

Table 2
Parameters and results of LCF tests at $R_d = -1$.

Test	Displacement amplitude d_a [mm]	Test frequency f [Hz]	Number of cycles N_i	Failed plate	Failure zone
A	0,2	5	60,000	Lower	Toe plate
B	0,35	5	2000	Upper	Toe plate
C	0,3	5	3300	Lower	Toe fillet
D	0,25	5	9000	Upper	Toe fillet
E	0,325	5	4500	Lower	Toe plate

Table 3
Parameters and results of LCF tests at $R_d = 0$.

Test	Displacement amplitude d_a [mm]	Test frequency f [Hz]	Number of cycles N_i	Failed plate	Failure zone
F	0,4	5	2350	Upper	Toe plate
G	0,5	5	850	Lower	Toe fillet
H	0,45	5	1450	Upper	Toe plate
I	0,55	5	360	Upper	Toe fillet
L	0,35	5	4050	Lower	Toe plate

[37].

The images of the specimens during the tests were acquired and processed by means of the ARAMIS 3D 12 M system, produced by GOM gmbH, using the DIC technique. The entire experimental setup is shown in Fig. 4. The DIC technique [39,41,42] is a full-field non-contact measurement method, which allows the detection of displacement and strain fields, and can be used to monitor areas that are hard to analyze using traditional techniques such as strain gages. Two cameras with a resolution of 4000 × 3000 pixels, with a focal length of 50 mm, were used during the tests. The system accuracy for the strain measurement is up to 0,01%, while the highest acquisition frequency is 58 Hz at the highest resolution. The specimens were coated with the aim of obtaining a black-white speckle pattern.

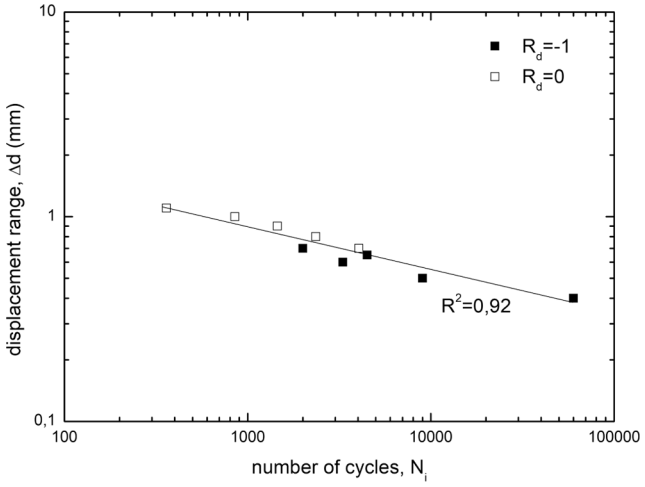

Fig. 5. Displacement amplitude d_a vs. fatigue life N_i (tests at $R_d = 0$ and $R_d = -1$).

2.2. Experimental results

Tables 2 and 3 report the parameters and the results of the tests performed at $R_d = -1$ and $R_d = 0$ respectively: test frequency (f), applied displacement amplitude (d_a) at the upper grip, experimental number of cycles to crack initiation (N_i) and failure location. The number of cycles (N_i) was assumed as the number of cycles to crack initiation, recorded when the maximum load decreased by 30% [43]. Toe fillet indicates that failure occurred in weld A or weld B, while toe plate indicates that failure occurred in weld C, as shown in Fig. 3(b) and 3(c).

Fig. 5 shows the applied displacement range $\Delta d - N_i$ curve. It is possible to note that both tests at $R_d = 0$ and $R_d = -1$ follow the same regression line, meaning that there is not significant influence of the different mean strain values on the LCF life. It is known that, as reported in [44], the effect of mean strain on strain range is small for a number of cycles N to fracture higher than 10 and for most strain-range values. Further studies [45] confirmed that the mean strain does not have an

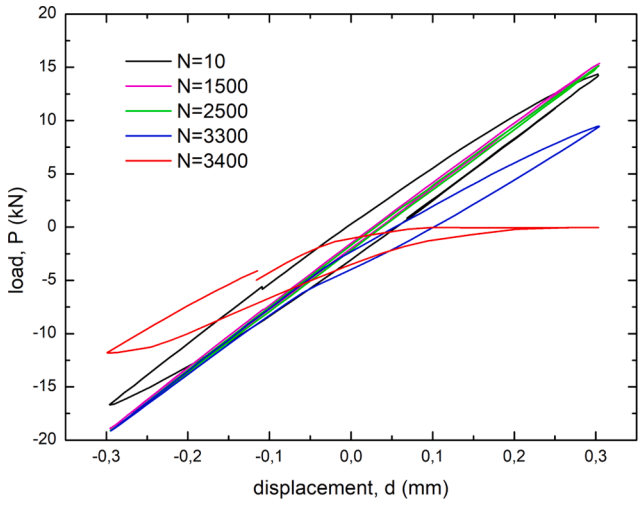

Fig. 6. Hysteresis cycles during test "C", d_a = 0,3 mm, R_d = -1.

effect on LCF life, if not complemented by half-life mean stress. As stated by Zhang et al. [46], the strain ratio effect on the mean stress is not significant for high strain ranges. Furthermore, it is described in [46] that there is a mean stress relaxation effect with increasing strain amplitude, typical of LCF tests, and the half-life mean stress goes to a stable value around zero.

Fig. 6 shows the most representative hysteresis cycles (applied displacement d vs load P) of test C (R_d = -1, d_a = 0,3 mm). At the beginning of the LCF tests, after few cycles necessary for obtaining the stable hysteresis cycle, the measured load range is almost constant. The hysteresis loop is almost constant until 2500 cycles, then it starts reducing. A load drop of 30 % is recorded around 3300 cycles.

All experimental tests were complemented by the DIC technique to monitor local areas.

Fig. 7 shows the map of the longitudinal strain (x-strain) on the surface during test "D" (d_a = 0,25 mm, R_d = -1), recorded by the DIC cameras, in correspondence of maximum and minimum applied displacements.

Some points, called "Stage Points" (SP) were introduced for the DIC analysis. The distance between each two consecutive SP is 5 mm and are shown in Fig. 8.

Fig. 9 shows the evolution of the longitudinal strain (x-strain) after 200 cycles of the different stage points. The upper plate is subjected to higher strain, shown in Fig. 9(a), while the lower plate has smaller values of strain, shown in Fig. 9(b). Moreover, mean values of the strain ranges of the different SP are slightly shifted towards positive values while getting closer to the weld toes, so there is an increment of the maximum strain, while the strain range has no significant change.

Fig. 10 shows the map of the longitudinal strain in correspondence of maximum and minimum applied displacements of test "H" ($R_d = 0$, d_a = 0,45 mm). The most strained plate is the upper plate from where the displacement is applied. However high strains extend also in the base material and not only in the proximity of the weld toe. In addition small values of compressive strains are detected, especially far from the weld toe, at minimum applied displacement, probably due to residual strain and/or by the pressure of the grips on the specimen.

From Fig. 11, which shows the longitudinal strain range evolution after 200 cycles, it is possible to see that the upper plate is subjected to higher strain, shown in Fig. 10(a), while the lower plate has smaller values of strain, shown in Fig. 10(b). The results, shown in Fig. 11, are similar to the ones obtained for R_d = -1 (Fig. 9): mean values of the strain ranges of the different SP are shifted towards positive values while getting closer to the weld toes, so there is an increment of the maximum strain, while the strain range has no significant change.

It is well known that the notch is characterized by a multiaxial stress/strain state. On the contrary of traditional experimental techniques as strain gauges, the 3D DIC technique and ARAMIS software allow evaluating the strain field in proximity of stress concentration zones. Thus a notch strain range ($\Delta\varepsilon_{n\_DIC}$), in terms of principal strain range, was evaluated in correspondence of the notch by means of DIC analysis.

Furthermore, it is recognized that weld notch radii differ in the same plate and could vary from large to very small values. For this reason, some numerical local approaches provide solutions considering a fictitious radius of 1 mm in order to evaluate the notch stress/strain values using FEA [3,26]. However, it has to be noted that the analyzed specimens have a toe radius close to 1 mm. The $\Delta\varepsilon_{n\_DIC}$ parameter was evaluated in correspondence of the notch at the midsection of the specimen, then it was correlated to the number of cycles in order to obtain and experimental $\Delta\varepsilon_{n\_DIC}$ - N curve, shown in Fig. 12.

It is remarkable to note that the experimental tests at both displacement ratios (R_d = -1 and R_d = 0) follow the same regression line, confirming that not significant effects of the different displacement ratios were observed on the LCF life.

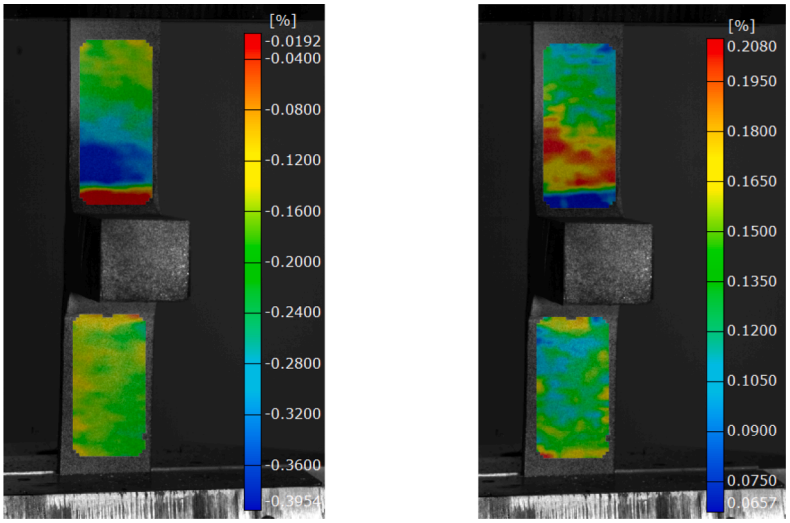

(a) minimum applied displacement (b) maximum applied displacement

Fig. 7. Longitudinal strain at minimum (a) and maximum (b) applied displacements, (test "D", d_a = 0,25 mm, R_d = -1).

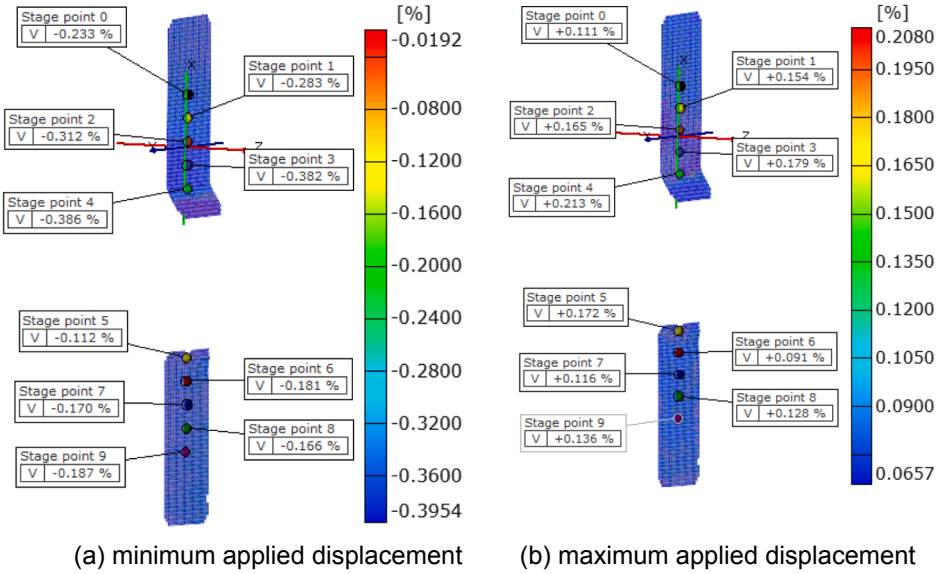

Fig. 8. 3D map and SP values of the longitudinal strain at minimum (a) and maximum (b) displacements (test "D", d_a = 0,25 mm, R_d = -1).

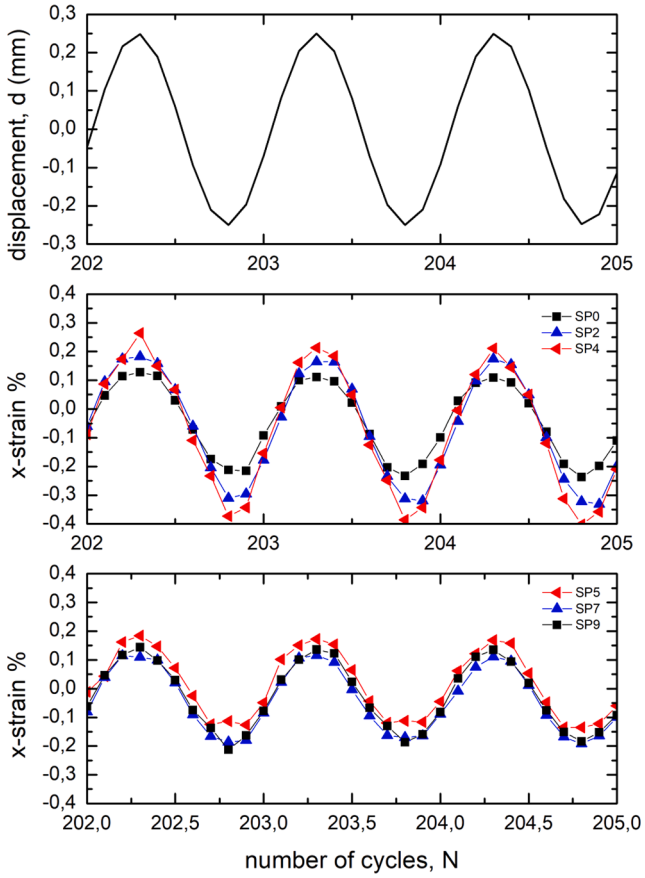

Fig. 9. Evolution of the longitudinal strain of the different Stage Points after 200 cycles (test "D", d_a = 0,25 mm, R_d = -1).

3. Equivalent structural strain approaches

3.1. Finite Element equivalent structural strain approach

Recently Pei and Dong proposed a structural strain parameter, which overcomes the strain singularity at weld toe, by characterizing the through thickness strain distribution, and has shown to be capable of correlating both LCF and HCF fatigue data of welded structures [31,32].

The structural strain parameter is computed by the analysis of the FE results. The structural strain definition is consistent with the traction structural stress definition adopted in the ASME Div2 code [30] in 2007. Both structural stress method and structural strain method are

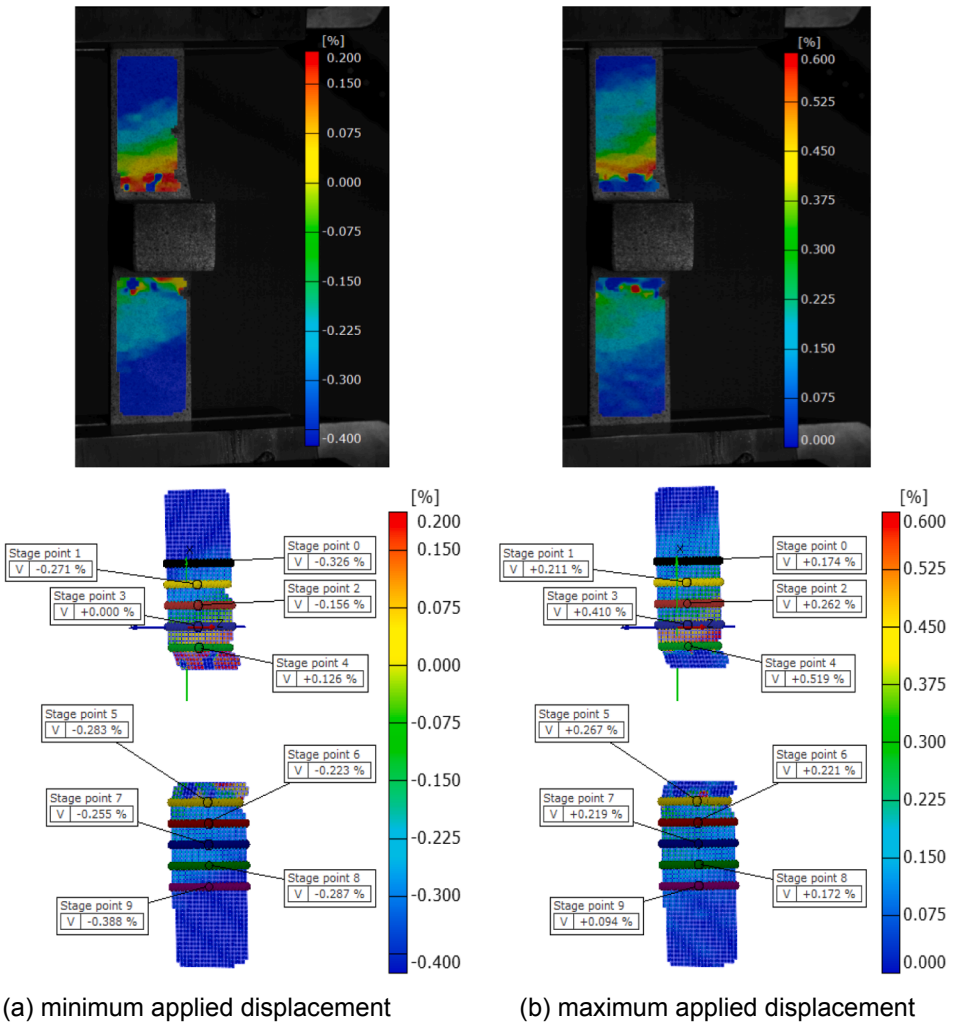

Fig. 10. 3D map and SP values of the longitudinal strain at minimum (a) and maximum (b) applied displacements (test "H", d_a = 0,45 mm).

specifically developed for the analysis of fatigue behavior of welded components with ill-defined notch radii at specific weld locations such as weld toe [4,28-32]. The structural strain method is an extension of the mesh-insensitive traction structural stress method [4,29,30] in which structural strain in terms of membrane and bending component is evaluated by means of the corresponding traction stress components. Fig. 13 schematically illustrates the structural strain definition.

Fig. 13(a) shows the cross-section of a fillet welded plate structure and a weld toe fatigue cracking into plate thickness, i.e., along Plane A-A, is considered. Although local stress along the hypothetical crack plane can be highly nonlinear, the corresponding traction structural stress component (i.e., opening stress component with respect crack plane A-A) can be evaluated through FEA under specified remote loading conditions. The traction stress is mesh-insensitive [4,30] and is expressed in terms of normal membrane part (σ_m) and normal bending part (σ_b). Then, an equivalent 2D plate section problem can be described as shown in Fig. 13b, subjected to the same statically equivalent membrane (σ_m) and bending stress (σ_b), as a function of the bending moment (M) and tensile load (N). The resulting linear strain distribution (linear deformation gradient) in terms of membrane strain (ϵ_m) and bending strain (ϵ_b) is defined as structural strain, which can be solved by imposing both equilibrium conditions and material yield criteria.

The overall procedure to determine the structural strain is provided in Fig. 14.

Firstly a FE of the welded joint, based on a linear elastic model, is performed, then the traction stress is evaluated and the critical location, where this stress has the highest value, is defined. Finally the structural strain is evaluated at this critical location. It is worth noting that in performing structural stress calculations, there is no need to introduce an artificial weld radius or special mesh refinement in the FE model.

The nodal forces are extracted by FE model along the weld, both at fillet and plate position. The corresponding membrane and bending stress are calculated using the following equation:

$$\sigma_m = \frac{\sum_{i=1}^{n_{node}} F_i}{t} \tag{1}$$

$$\sigma_b = \frac{6\sum_{i=1}^{n_{node}} F_i(y_i - t/2)}{t^2} \tag{2}$$

F_i and y_i represents the nodal force and y coordinate at the *ith* node in the Eqs. (1) and (2) respectively, while t is the thickness of the plate.

Using the traction stress, evaluated from Eqs. (1) and (2), the corresponding structural strain (ϵ_s) can be calculated according to the procedure reported in [31,32].

The traction structural stresses are computed under given fatigue loading conditions and, if they exceed the material yield condition, the structural strain should be calculated by postprocessing the nonlinear FE model to obtain the traction stress first, and use the iterative approach, recently given in [32], for determining the corresponding structural strains for Ramberg-Osgood power law hardening material behavior. Otherwise, the structural strain can be simply related to the traction structural stresses calculated by means of the constitutive equations for

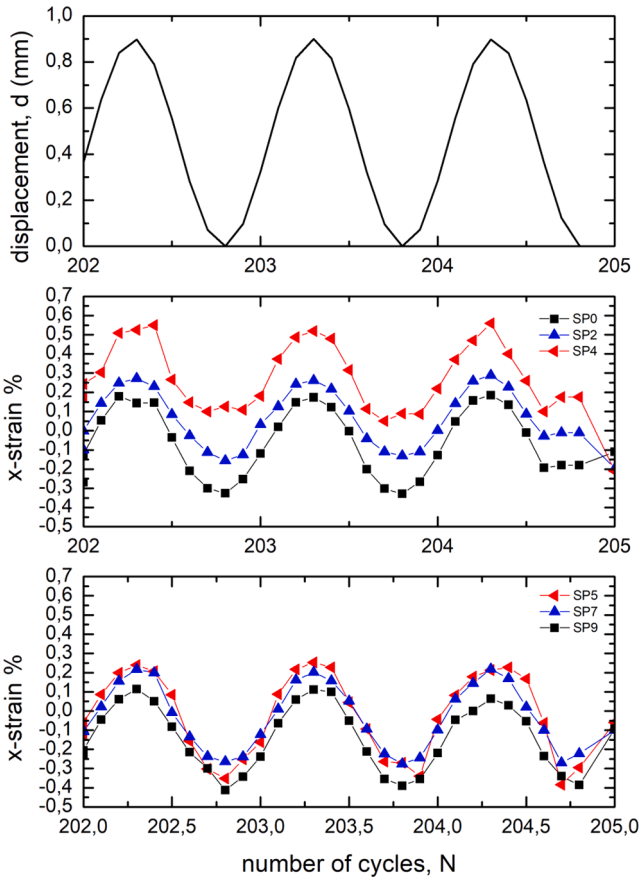

Fig. 11. Longitudinal strain at stage points (test "H", d_a = 0,45 mm, R_d = 0).

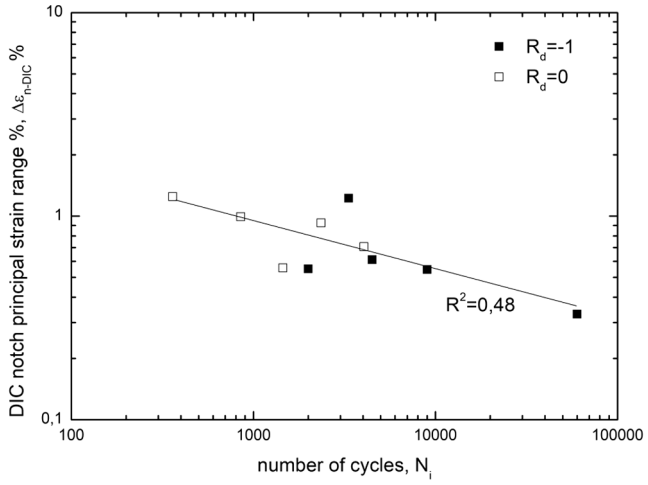

Fig. 12. $\Delta\varepsilon_{n\_DIC}$ - N curve, tests at R_d = 0 and R_d = -1.

plane strain conditions, as:

$$\epsilon_m = \frac{\sigma_m(1-\nu^2)}{E} \tag{3}$$

$$\epsilon_b = \frac{\sigma_b(1-\nu^2)}{E} \tag{4}$$

$$\epsilon_s = \epsilon_m + \epsilon_b \tag{5}$$

However, it is worth to mention that, according to [31,47], if the experimental tests are performed under displacement control condition, the structural strain can even be calculated through a linear elastic model using Eqs. (3) and (4). The difference between the structural strain values, calculated by nonlinear and linear FE models, is not significant because the structural strain captures the through thickness average effect. The average strain information shows no significant difference under displacement control condition, since the deformation is directly applied. Detailed discussion on this topic can be found in Ref [32,47].

Once the structural strain ($\Delta\epsilon_s$) is obtained, the equivalent structural strain (ΔE_s) can be calculated for fatigue evaluation. The equivalent structural strain is given as:

$$\Delta E_s = \frac{\Delta\epsilon_s}{t^{*\frac{2-m}{2m}} I(r)^{1/m}} \tag{6}$$

$$r = \frac{\epsilon_b}{\epsilon_m + \epsilon_b} \tag{7}$$

$$t^* = t/t_{ref}, t_{ref} = 1mm \tag{8}$$

$$I(r)^{1/m} = 0.0011r^6 + 0.0767r^5 - 0.0988r^4 + 0.0946r^3 + 0.0221r^2 + 1.2223 \tag{9}$$

Where the life integral *I(r)* is a dimensionless function of bending ratio *r* and $m = 3.6$ is calculated in previous works from fracture mechanics considerations [30].

Then, the experimental value of the fatigue life is plotted against the equivalent structural strain range (ΔE_s) and compared with master E-N curve. The master E-N curve is converted from the ASME Div 2 master S-N curve representing over 1000 large scale fatigue tests, where large scale is defined when the ratio width to thickness W/t>=10 [30], with the number of cycles to failure ranging from 10^2 to 10^8 cycles. There are

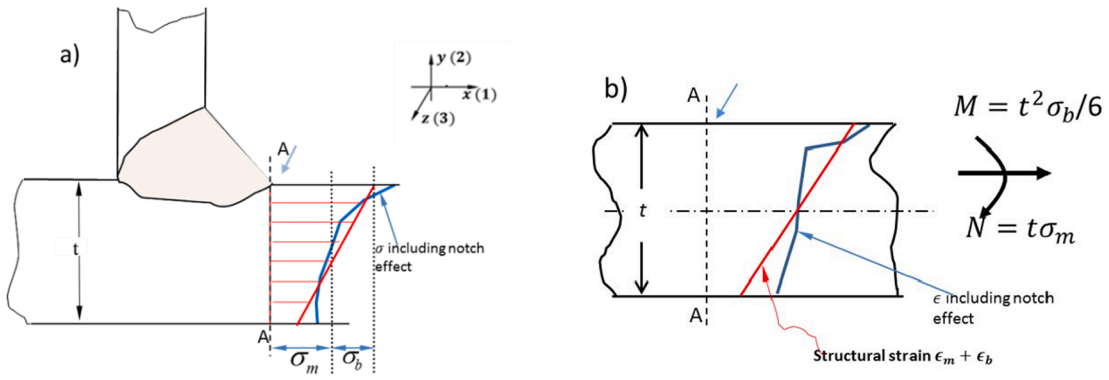

Fig. 13. Structural strain definitions: a) Traction structural stress ($\sigma_m + \sigma_b$) determined on a plate cross-section A-A using the mesh-insensitive method [30]; b) structural strain (ϵ_m, ϵ_b) at along plate section A-A.

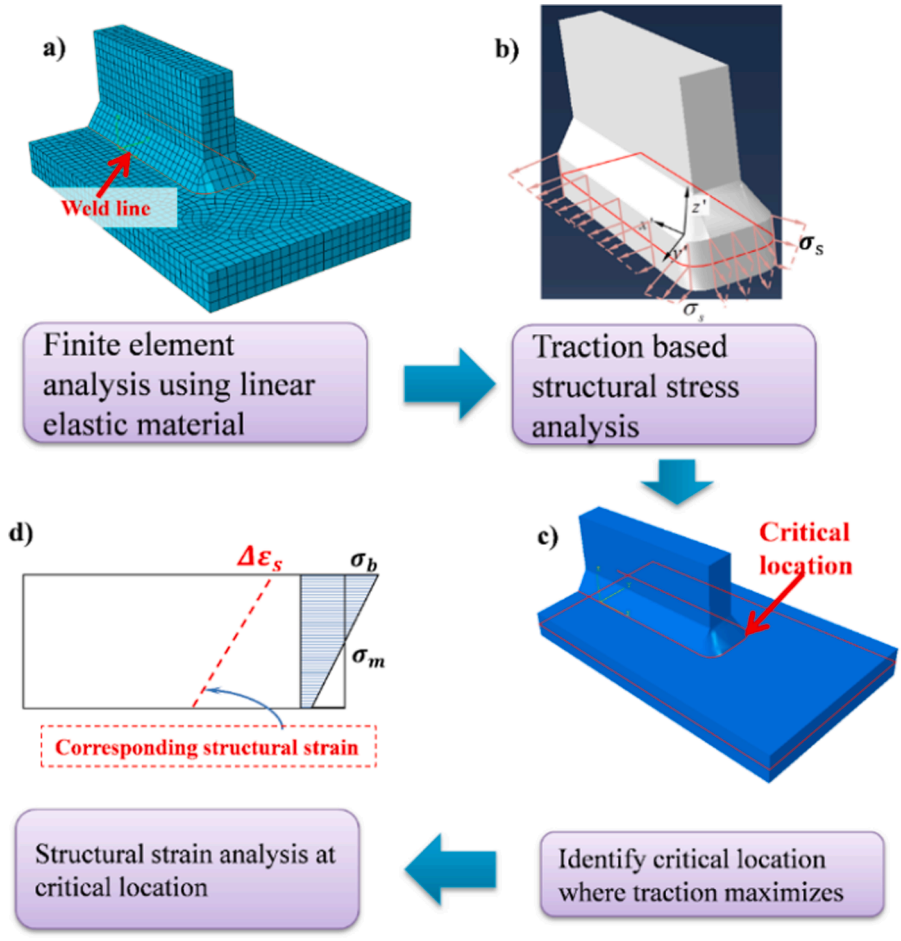

Fig. 14. Overall procedure of structural strain analysis: a) Perform FEA using linear elastic model. b) Conduct traction-based structure stress analysis along weld line. c) Identify critical location where traction stress maximizes. d) Calculate the structural strain at the critical location.

two Master S-N curves in ASME code, one for steel, and one for aluminium. However, as shown in [31], when LCF fatigue data are analyzed using the structural strain approach, fatigue data of different metals can be collapsed in a single master E-N curve. The validation was already shown in a recent work by some of the authors [31]. The fatigue life predicted by the master E-N curve implies local through-thickness failure criterion.

A two-dimensional (2D) plane-strain FE model of the investigated AA5083 welded joint was performed for evaluating the through thickness structural strain parameter.

The FEA was performed by means of the commerical FE software ABAQUS, using CPE4 element type. Due to the symmetry of the sample, only half of the investigated welded joint was modelled. The loading and boundary conditions are shown in Fig. 15. The displacement along *y* direction was fixed to simulate the grip condition during the tests, and a gap was modeled to simulate the lack of penetration.

As reported above, there is no need to introduce an artificial weld radius or special mesh refinement in the FE model for evaluating the structural stress.

Furthermore, since the specimen is dominantly under normal strain,

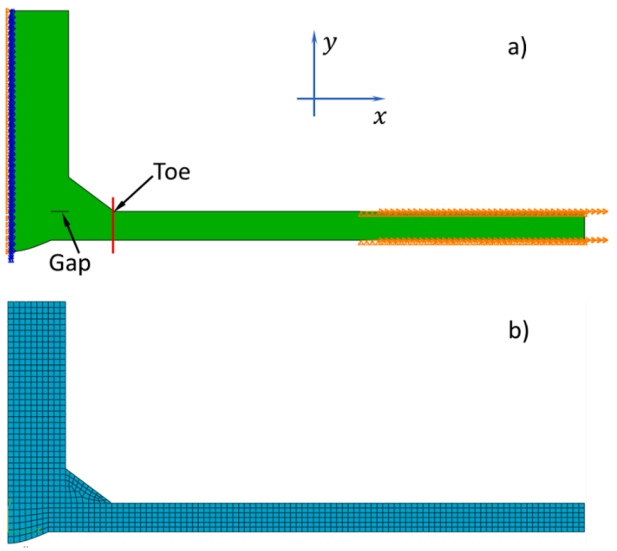

Fig. 15. a) Loading and boundary conditions of the FE model; b) Mesh of the FE model.

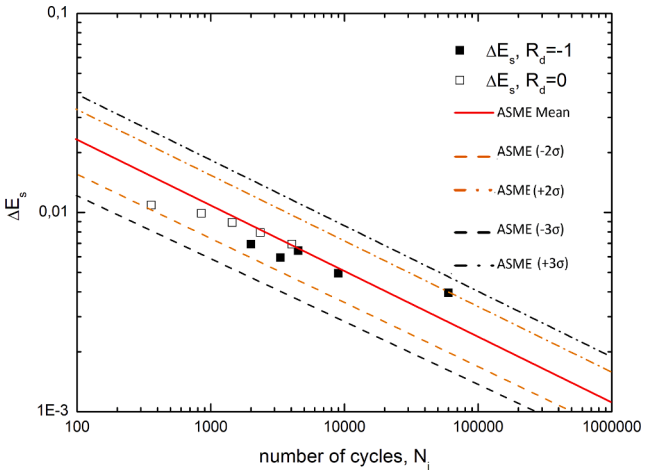

Fig. 16. Comparison of the FE results with ASME Div Master E-N curve scatter band in terms of equivalent structural strain range.

Table 4
Parameters of Master E-N curve.

Statistical Basis	*C*	*h*
Mean Curve	0.10434	0.32748
Upper 95% prediction interval (+2σ)	0.16838	0.32748
Lower 95% prediction interval (-2σ)	0.06465	0.32748
Upper 99% prediction interval (+3σ)	0.27174	0.32748
Lower 99% prediction interval (-3σ)	0.04006	0.32748

due to the actual loading conditions, the effect of shear component is neglected in this study. Indeed the FEA reveals that the ratio of traction shear stress and normal stress at the toe fillet is $\tau_m/\sigma_m \approx 10^{-8}$.

According to the procedure described above, the nodal forces are extracted along the weld, both at fillet and plate position, as indicated using the red line in Fig. 15(a), then the values of membrane and bending stress are evaluated according to the Eqs (1) and (2), and finally the values of the corresponding structural strain can be evaluated.

As observed experimentally in Table 2, failure occurred sometimes in the toe fillets (welds A and B) and sometimes in the toe plate (weld C). The FE structural strain values, calculated in the toe fillet and in the toe plate, give both similar results. For this reason, and because the experimental DIC technique allowed evaluating the local strain values just from one side of the specimen, only the toe fillet equivalent structural strain values are used for comparison. Then the experimental values of the LCF lives are plotted against the equivalent structural strain range and compared with master E-N curve in Fig. 16.

It is worth noting that overall comparison of the tested fatigue data, at R_d = -1, agrees with the ASME curve.

Fig. 16 shows that the experimental data, obtained by LCF tests at R_d = 0, are close to the ASME Mean curve and lie inside the $\pm 2\sigma$ boundary of the design curves.

The fatigue life of the welded specimen can be predicted using the following equation:

$$\Delta E_s = C \times N^{-h} \tag{17}$$

in which ΔE_s is given in Eq. (6).

The parameters C and h of Eq. (7), relative to the Master E-N curve, are given in Table 4.

3.2. Digital Image Correlation equivalent structural strain approach

Firstly, the structural strain range ($\Delta\epsilon_{s-DIC}$) was evaluated on the line path (red line of Fig. 17) of the specimen surface by means of the experimental strain values, obtained by DIC analysis. The same figure also shows the longitudinal strain map.

The distance from each weld toe, indicated as x in Fig. 17, was normalized by the thickness (t) of the plate. The percentage longitudinal strain vs x/t ratio was obtained for each test.

The structural strains (ϵ_{s-max} and ϵ_{s-min}) were evaluated at midlife of each test as the strain values at weld toe (x = 0), obtained by means of the linear regression of the strain values between 1 t and 2 t, corresponding respectively at maximum and minimum applied displacements (d_{max} and d_{min}) as shown in Fig. 18.

As an example, the strain distribution for test performed at R_d = -1 and R = 0 are shown respectively in Figs. 19 and 20.

The structural strains are used to calculate the structural strain range $\Delta\epsilon_{s-DIC}$ as:

$$\Delta\epsilon_{s-DIC} = \epsilon_{s-max} - \epsilon_{s-min} \tag{18}$$

The obtained parameters are shown in Tables 5 and 6. The structural strain values were evaluated in the plate where failure occurred, which is the one producing the maximum $\Delta\epsilon_{s-DIC}$. These values were used for the$\Delta\epsilon_{s-DIC}$– **N** curve.

Fig. 21 shows the structural strain range ($\Delta\epsilon_{s-DIC}$%), evaluated from DIC analysis, vs number of cycles (N_i). It is interesting to note that the LCF tests at both displacement ratios (R_d = 0 and R_d = -1) follow the same regression line.

Once the structural strain $\Delta\epsilon_{s-DIC}$is obtained, the DIC equivalent structural strain (ΔE_{s_DIC}) can be evaluated according to the following equation:

$$\Delta E_{s\_DIC} = \frac{\Delta\epsilon_{s\_DIC}}{t^{\frac{s2-m}{2m}} I(r)^{1/m}} \tag{19}$$

As mentioned above, the parameter (m) is calculated in previous works from fracture mechanics considerations (m = 3.6) and the life integral *I(r)* is a dimensionless function of the bending ratio *(r)*, which depends on the bending and membrane strains (ϵ_b. and ϵ_m).

The values of bending and membrane strains (ϵ_b. and ϵ_m) were evaluated by FE and experimental analyses in order to compare the results.

At a first attempt, the same values of *I(r)* were assumed for DIC and FE equivalent structural strains where ϵ_b and ϵ_m were evaluated by FEA.

Table 7 shows the values of DIC and FE equivalent structural strains (ΔE_s and ΔE_{s_DIC}) at toe fillet. The ΔE_{s_DIC} values, reported in Table 7,

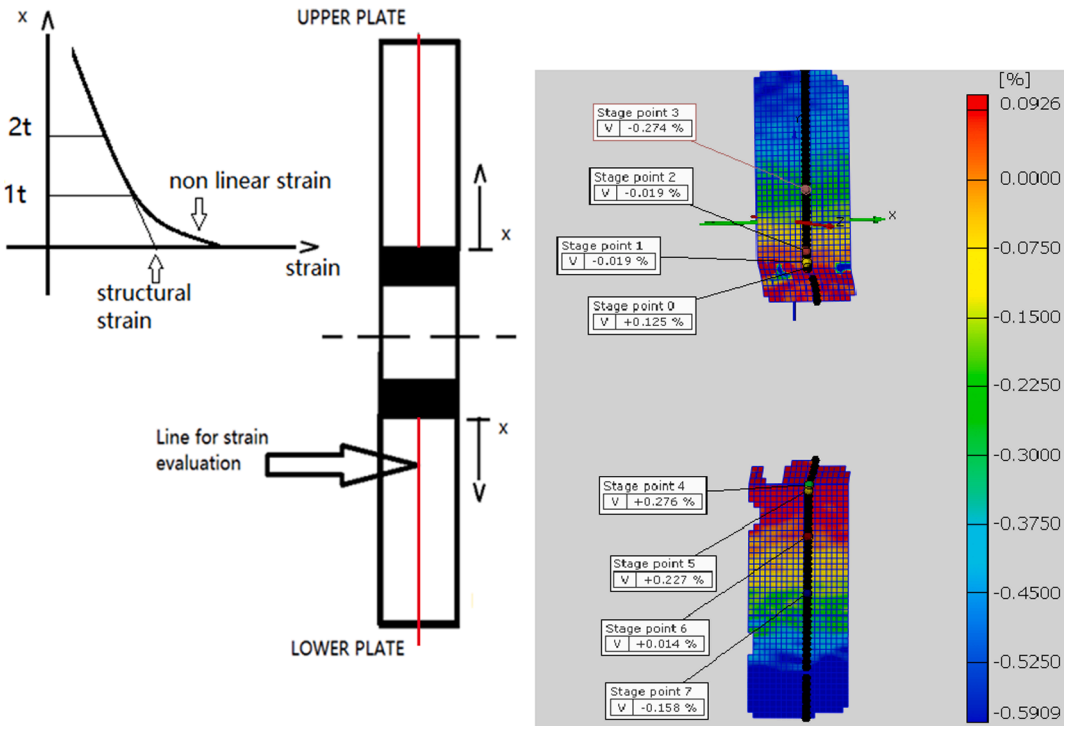

Fig. 17. (a) Structural strain and line path definition, (b) DIC longitudinal strain map and line path at the midsection for structural strain evaluations.

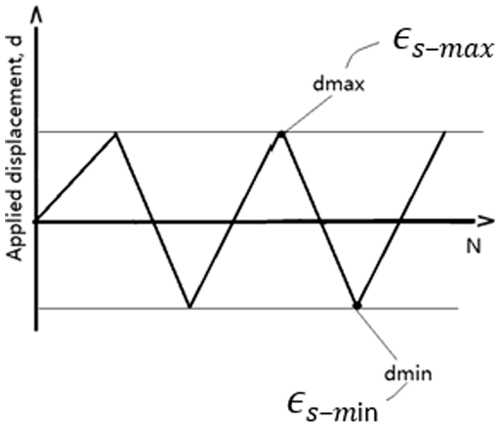

Fig. 18. Structural strains considered at maximum and minimum values of applied displacement.

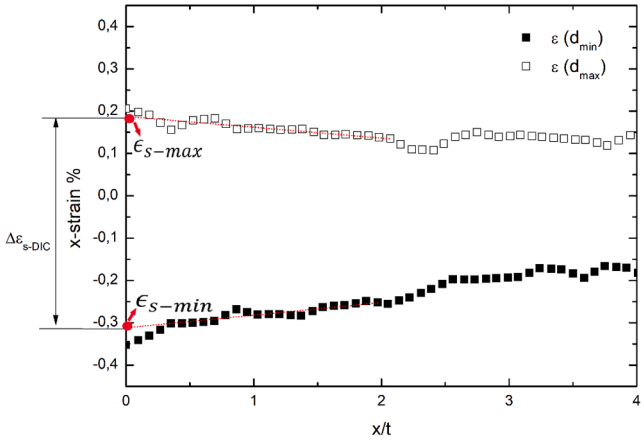

Fig. 19. DIC structural strain for test "D", d_a = 0,25 mm, R_d = -1.

were evaluated in the plate (upper or lower plate of the welded joint) where the maximum $\Delta\epsilon_{s-DIC}$ and failure occurred.

Fig. 22 shows the DIC and FE equivalent structural strains (ΔE_s and ΔE_{s_DIC}) compared to the ASME curve (red curve). It is interesting to note that, although a slightly higher dispersion, the values of the DIC equivalent structural strain (ΔE_{s_DIC}), calculated on the surface of the specimen, falls inside the $\pm$ 3σ scatter bands (outer bands).

Alternatively, in order to propose a complete independent experimental procedure, $I(r)$ was calculated directly, from the experimental values of bending and membrane strains (ϵ_b and ϵ_m) evaluated by DIC analyses, assuming that $\epsilon_m = \Delta d/2L$, where L is the distance between the grip and the fillet weld toe ($L = 94mm$). Then, the DIC equivalent structural strain (ΔE_{s_DIC}), evaluated from independent experimental measurements, and FE equivalent structural strain (ΔE_s) can be compared to the ASME curve, as shown in Fig. 23. It is interesting to note that also in this case DIC equivalent structural strains (ΔE_{s_DIC}) fall inside the $\pm$ 3σ scatter bands. Fig. 23 demonstrated the effectiveness of the adopted experimental procedure, for the DIC equivalent structural strain evaluations, and further confirmed the reliability of the FE equivalent structural strain approach.

4. Conclusions

LCF tests of welded specimens made of Al 5083 have been performed under displacement control and the following conclusions can be drawn:

- The DIC equivalent structural strains (ΔE_{s_DIC}) and FE equivalent structural strains (ΔE_s) were compared to the ASME curve, showing the effectiveness of the adopted experimental procedure and further confirming the reliability of the equivalent FE structural strain approach.
- The experimental data for LCF tests at both displacement ratios (R_d = -1 and R_d = 0) follow the same regression line, indicating no significant effects of the different displacement ratios R_d on LCF life.

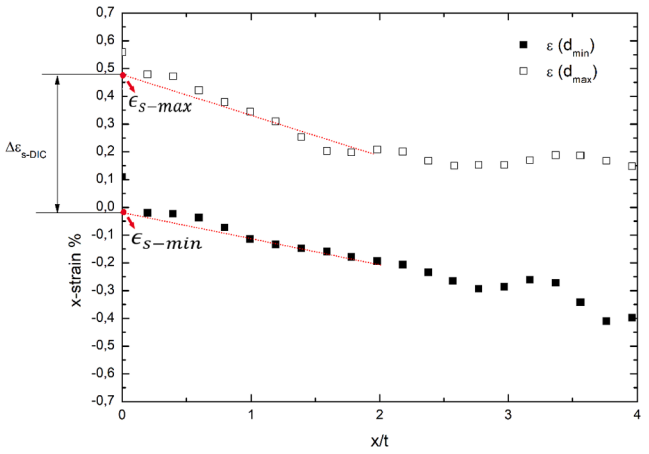

Fig. 20. DIC structural strain for test "H", d_a = 0,45 mm, R_d = 0.

Table 5
DIC structural strain values for test at R_d = -1.

Test	d_a (mm)	N_i	$\Delta\epsilon_{s-DIC}$%	failed plate
A	0,2	60,000	0,287	Lower
B	0,35	2000	0,4784	Upper
C	0,3	3330	0,91	Lower
D	0,25	9000	0,5095	Upper
E	0,325	4500	0,5209	Lower

- By applying the linear and mesh insensitive structural strain approach, LCF test data can be compared with ASME Div 2 master E-N curve representing over 1000 large scale fatigue tests with number of cycles to failure ranging from 10^2 to 10^8. The LCF tests carried out fall inside the $\pm 2\sigma$ boundary of the design curves.

Table 6
DIC structural strain values for test at R_d = 0.

Test	d_a (mm)	N_i	$\Delta\epsilon_{s-DIC}$%	failed plate
F	0,4	2350	0,724	Upper
G	0,5	850	0,9957	Lower
H	0,45	1450	0,5195	Upper
I	0,55	360	0,8596	Upper
L	0,35	4050	0,6224	Lower

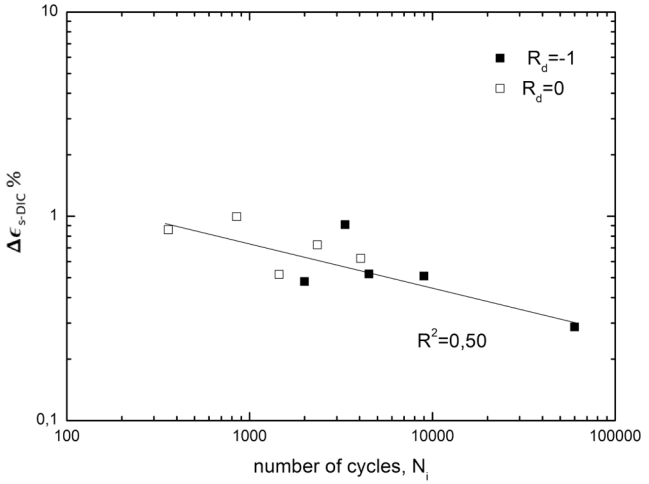

Fig. 21. $\Delta\epsilon_{s-DIC}$– N_i curve.

Table 7
DIC and FE equivalent structural strains at toe fillet.

Test #	Δd [mm]	ΔE_s	ΔE_{s_DIC}
5	0,6	5,94E-03	1,06E-02
6	0,5	4,95E-03	5,71E-03
2	0,4	3,96E-03	3,35E-03
4	0,7	6,93E-03	5,59E-03
10	0,65	6,43E-03	6,09E-03
11	0,8	7,92E-03	8,46E-03
12	1	9,90E-03	1,16E-02
13	0,9	8,91E-03	6,07E-03
14	1,1	1,09E-02	1,00E-02
15	0,7	6,93E-03	7,27E-03

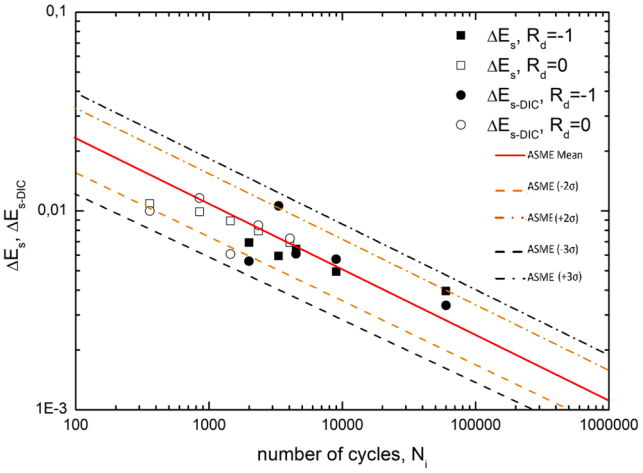

Fig. 22. ΔE_s and ΔE_{s_DIC} compared to the ASME curve ($I(r)$ was evaluated from FEA also for ΔE_{s_DIC}).

- Completely independent experimental procedure to evaluate the DIC equivalent structural strain was proposed for the first time.
- The 3D analyses carried out by DIC allowed obtaining the DIC notch strain range ($\Delta\varepsilon_{n\text{-}DIC}$), in terms of principal strain range, in correspondence of the notch. Then it was correlated to the number of cycles, obtaining the $\Delta\varepsilon_{n\text{-}DIC}$ - N_i curve. The proposed approach could be a powerful tool for the evaluation of a new experimental master curve, expressed in terms of $\Delta\varepsilon_{n\_DIC}$ and considering different weld geometries and boundary/loading conditions.

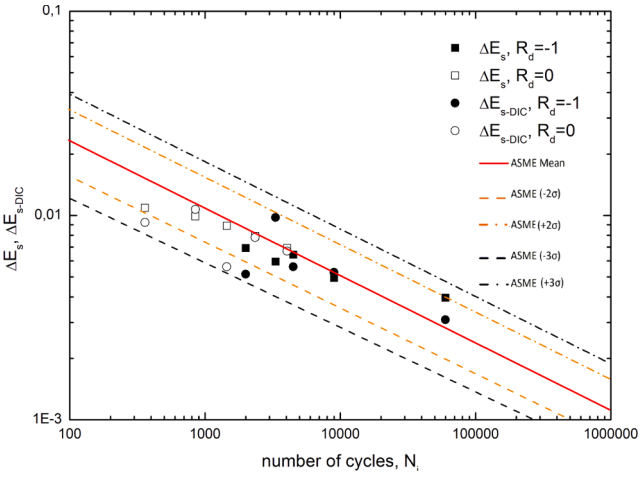

Fig. 23. ΔE_s and ΔE_{s_DIC} compared to the ASME curve ($I(r)$ was evaluated experimentally for ΔE_{s_DIC}).

Declaration of Competing Interest

The authors declare that they have no known competing financial interests or personal relationships that could have appeared to influence the work reported in this paper.

References

[1] W. Fricke, Recent developments and future challenges in fatigue strength assessment of welded joints, Proc. Inst. Mech. Eng. Part C J. Mech. Eng. Sci. 229 (7) (2015) 1224–1239, https://doi.org/10.1177/0954406214550015.

[2] B. Atzori, P. Lazzarin, G. Meneghetti, Fatigue strength of welded joints based on local, semi-local and nominal approaches, Theor. Appl. Fract. Mech. 52 (1) (2009) 55–61, https://doi.org/10.1016/j.tafmec.2009.06.006.

[3] D. Radaj, C.M. Sonsino, W. Fricke, Recent developments in local concepts of fatigue assessment of welded joints, Int. J. Fatigue. 31 (2009) 2–11. Doi: 10.1016/j.ijfatigue.2008.05.019.

[4] P. Dong, A structural stress definition and numerical implementation for fatigue analysis of welded joints, Int. J. Fatigue. 23 (2001) 865–876, https://doi.org/10.1016/S0142-1123(01)00055-X.

[5] D. Radaj, C.M. Sonsino, W. Fricke, Fatigue Assessment of Welded Joints by Local Approaches: Second Edition, Elsevier Ltd, 2006. Doi: 10.1533/9781845691882.

[6] C.M. Sonsino, D. Radaj, U. Brandt, H.P. Lehrke, Fatigue assessment of welded joints in AlMg 4.5Mn aluminum alloy (AA 5083) by local approaches, Int. J. Fatigue. 21 (1999) 985–999, https://doi.org/10.1016/S0142-1123(99)00049-3.

[7] P. Lazzarin, R. Tovo, A notch intensity factor approach to the stress analysis of welds, Fatigue Fract. Eng. Mater. Struct. 21 (9) (1998) 1089–1103, https://doi.org/10.1046/j.1460-2695.1998.00097.x.

[8] B. Atzori, P. Lazzarin, G. Meneghetti, M. Ricotta, Fatigue design of complex welded structures, Int. J. Fatigue. 31 (1) (2009) 59–69, https://doi.org/10.1016/j.ijfatigue.2008.02.013.

[9] D. Taylor, Geometrical effects in fatigue: a unifying theoretical model, Int. J. Fatigue. 21 (5) (1999) 413–420, https://doi.org/10.1016/S0142-1123(99)00007-9.

[10] D. Taylor, N. Barrett, G. Lucano, Some new methods for predicting fatigue in welded joints, Int. J. Fatigue. 24 (2002) 509–518, https://doi.org/10.1016/S0142-1123(01)00174-8.

[11] D. Taylor, The theory of critical distances: a new perspective in fracture mechanics, Elsevier, 2007.

[12] D. Taylor, The Theory of Critical Distances: A link to micromechanisms, Theor. Appl. Fract. Mech. 90 (2017) 228–233, https://doi.org/10.1016/J.TAFMEC.2017.05.018.

[13] V. Crupi, E. Guglielmino, A. Risitano, D. Taylor, Different methods for fatigue assessment of T welded joints used in ship structures, J. Sh. Res. 51 (2007) 150–159, https://doi.org/10.5957/jsr.2007.51.2.150.

[14] L. SUSMEL, Modified Wöhler curve method, theory of critical distances and Eurocode 3: A novel engineering procedure to predict the lifetime of steel welded joints subjected to both uniaxial and multiaxial fatigue loading, Int. J. Fatigue. 30 (5) (2008) 888–907, https://doi.org/10.1016/j.ijfatigue.2007.06.005.

[15] J.L. Fan, X.L. Guo, C.W. Wu, Y.G. Zhao, Research on fatigue behavior evaluation and fatigue fracture mechanisms of cruciform welded joints, Mater. Sci. Eng. A. 528 (29-30) (2011) 8417–8427, https://doi.org/10.1016/j.msea.2011.08.037.

[16] P. Williams, M. Liakat, M.M. Khonsari, O.M. Kabir, A thermographic method for remaining fatigue life prediction of welded joints, Mater. Des. 51 (2013) 916–923, https://doi.org/10.1016/j.matdes.2013.04.094.

[17] X.G. Wang, V. Crupi, C. Jiang, E. Guglielmino, Quantitative Thermographic Methodology for fatigue life assessment in a multiscale energy dissipation framework, Int. J. Fatigue. 81 (2015) 249–256, https://doi.org/10.1016/j.ijfatigue.2015.08.015.

[18] G. La Rosa, A. Risitano, Thermographic methodology for rapid determination of the fatigue limit of materials and mechanical components, Int. J. Fatigue. 22 (2000) 65–73, https://doi.org/10.1016/S0142-1123(99)00088-2.

[19] J. Fan, X. Guo, C. Wu, V. Crupi, E. Guglielmino, Influence of heat treatments on mechanical behavior of FV520B steel, Exp. Tech. 39 (2) (2015) 55–64, https://doi.org/10.1111/ext.2015.39.issue-210.1111/ext.12019.

[20] P. Corigliano, V. Crupi, Fatigue analysis of TI6AL4V / INCONEL 625 dissimilar welded joints, Ocean Eng. 221 (2021) 108582, https://doi.org/10.1016/j.oceaneng.2021.108582.

[21] L. Carteron, C. Doudard, S. Calloch, B. Levieil, J. Beaudet, F. Bridier, Naval welded joints local stress assessment and fatigue cracks monitoring with quantitative thermoelastic stress analysis, Theor. Appl. Fract. Mech. 110 (2020) 102792, https://doi.org/10.1016/j.tafmec.2020.102792.

[22] P. LAZZARIN, F. BERTO, F. GOMEZ, M. ZAPPALORTO, Some advantages derived from the use of the strain energy density over a control volume in fatigue strength assessments of welded joints, Int. J. Fatigue. 30 (8) (2008) 1345–1357, https://doi.org/10.1016/j.ijfatigue.2007.10.012.

[23] P. Lazzarin, R. Zambardi, A finite-volume-energy based approach to predict the static and fatigue behavior of components with sharp V-shaped notches, Int. J. Fract. 112 (2001) 275–298, https://doi.org/10.1023/A:1013595930617.

[24] W. Shen, M. Zuo, S. Xu, E. Liu, Evaluation of fatigue strength of cruciform welded joints by strain energy density method based on singular strength factor, Theor. Appl. Fract. Mech. 108 (2020) 102639, https://doi.org/10.1016/j.tafmec.2020.102639.

[25] F. Berto, P. Lazzarin, A review of the volume-based strain energy density approach applied to V-notches and welded structures, Theor. Appl. Fract. Mech. 52 (3) (2009) 183–194, https://doi.org/10.1016/j.tafmec.2009.10.001.

[26] K. Saiprasertkit, Fatigue strength assessment of load-carrying cruciform joints in low- and high-cycle fatigue region based on effective notch strain concept: HENRY GRANJON PRIZE 2013 Winner Category C: Design and Structural Integrity, Weld. World. 58 (2014) 455–467. Doi: 10.1007/s40194-014-0129-8.

[27] M.D. Chapetti, L.F. Jaureguizahar, Fatigue behavior prediction of welded joints by using an integrated fracture mechanics approach, Int. J. Fatigue. 43 (2012) 43–53, https://doi.org/10.1016/j.ijfatigue.2012.02.004.

[28] P. Dong, X. Pei, S. Xing, M.H. Kim, A structural strain method for low-cycle fatigue evaluation of welded components, Int. J. Press. Vessel. Pip. 119 (2014) 39–51, https://doi.org/10.1016/j.ijpvp.2014.03.003.

[29] A. Hobbacher, RECOMMENDATIONS FOR FATIGUE DESIGN OF WELDED JOINTS AND COMPONENTS, IIW Doc. IIW-1823-07 Ex XIII-2151r4-07/XV-1254r4-07. (2008).

[30] P. Dong, American Society of Mechanical Engineers, The master S-N curve method: an implementation for fatigue evaluation of welded components in the ASME B & PV code, Section VIII, Division 2 and API 579–1/ASME FFS-1, Welding Research Council (2010).

[31] X. Pei, P. Dong, S. Xing, A structural strain parameter for a unified treatment of fatigue behaviors of welded components, Int. J. Fatigue. 124 (2019) 444–460, https://doi.org/10.1016/j.ijfatigue.2019.03.010.

[32] Xianjun Pei, Pingsha Dong, An analytically formulated structural strain method for fatigue evaluation of welded components incorporating nonlinear hardening effects, Fatigue Fract. Eng. Mater. Struct. 42 (1) (2019) 239–255, https://doi.org/10.1111/ffe.v42.110.1111/ffe.12900.

[33] Carole Erny, David Thevenet, Jean-Yves Cognard, Manuel Körner, Fatigue life prediction of welded ship details, Mar. Struct. 25 (1) (2012) 13–32, https://doi.org/10.1016/j.marstruc.2011.10.001.

[34] L. Feng, X. Qian, Low cycle fatigue test and enhanced lifetime estimation of high-strength steel S550 under different strain ratios, Mar. Struct. 61 (2018) 343–360, https://doi.org/10.1016/j.marstruc.2018.06.011.

[35] I. Gledić, J. Parunov, P. Prebeg, M. Ćorak, Low-cycle fatigue of ship hull damaged in collision, Eng. Fail. Anal. 96 (2019) 436–454, https://doi.org/10.1016/j.engfailanal.2018.11.005.

[36] R. Eriksson, J. Moverare, Z. Chen, A low cycle fatigue life model for a shot peened gas turbine disc alloy, Int. J. Fatigue. 124 (2019) 34–41, https://doi.org/10.1016/J.IJFATIGUE.2019.02.034.

[37] Bruno Levieil, Cédric Doudard, David Thevenet, Florent Bridier, Anthony Ezanno, Sylvain Calloch, Taking residual stresses into account in low-cycle fatigue design using the adjustable localisation operator method, Int. J. Fatigue. 150 (2021) 106322, https://doi.org/10.1016/j.ijfatigue.2021.106322.

[38] J.C. Kim, S.K. Cheong, H. Noguchi, Residual stress relaxation and low- and high-cycle fatigue behavior of shot-peened medium-carbon steel, Int. J. Fatigue. 56 (2013) 114–122, https://doi.org/10.1016/J.IJFATIGUE.2013.07.001.

[39] P. Corigliano, V. Crupi, E. Guglielmino, Non linear finite element simulation of explosive welded joints of dissimilar metals for shipbuilding applications, Ocean Eng. 160 (2018) 346–353, https://doi.org/10.1016/j.oceaneng.2018.04.070.

[40] P. Corigliano, M. Ragni, D. Castagnetti, V. Crupi, E. Dragoni, E. Guglielmino, Measuring the static shear strength of anaerobic adhesives in finite thickness under high pressure, J. Adhes. 97 (8) (2021) 783–800, https://doi.org/10.1080/00218464.2019.1704271.

[41] A. Sedmak, M. Milosevic, N. Mitrovic, A. Petrovic, T. Maneski, Digital image correlation in experimental mechanical analysis, Struct. Integr. Life (2012) 39–42.

[42] N. Milosevic, B. Younise, A. Sedmak, M. Travica, A. Mitrovic, Evaluation of true stress–strain diagrams for welded joints by application of Digital Image Correlation, Eng. Fail. Anal. 128 (2021) 105609, https://doi.org/10.1016/j.engfailanal.2021.105609.

[43] K. Saiprasertkit, E. Sasaki, C. Miki, Fatigue crack initiation point of load carrying cruciform joints in low and high cycle fatigue regions, Int. J. Fatigue. 59 (2014) 153–158, https://doi.org/10.1016/j.ijfatigue.2013.09.002.

[44] K. Ohji, W.R. Miller, J. Marin, Cumulative damage and effect of mean strain in low-cycle fatigue of a 2024–T351 aluminum alloy, J. Fluids Eng. Trans. ASME. 88 (1966) 801–809, https://doi.org/10.1115/1.3645963.

[45] S.K. Koh, R.I. Stephens, Mean stress effects on low cycle fatigue for a high strength steel, Fatigue Fract. Eng. Mater. Struct. 14 (4) (1991) 413–428, https://doi.org/10.1111/ffe.1991.14.issue-410.1111/j.1460-2695.1991.tb00672.x.

[46] Junhong Zhang, Weidong Li, Huwei Dai, Nuohao Liu, Jiewei Lin, Study on the elastic-plastic correlation of low-cycle fatigue for variable asymmetric loadings, Materials (Basel). 13 (11) (2020) 2451, https://doi.org/10.3390/ma13112451.

[47] Xianjun Pei, Pingsha Dong, Myung Hyun Kim, A simplified structural strain method for low-cycle fatigue evaluation of girth-welded pipe components, Int. J. Fatigue. 139 (2020) 105732, https://doi.org/10.1016/j.ijfatigue.2020.105732.